6. SURFACE FUNCTIONALIZATIONS, DRUG LOADING AND EVALUATIONS OF NANOPARTICLES

Table 6.1: List of chemicals used in the present work.

Sr. No.	Chemicals	Source and Place
1	(3-aminopropyl)triethoxysilane (APTES)	TCI chemicals, India
2	Succinic anhydride (SA)	Spectrochem Pvt. Ltd., India
3	N-hydroxysuccinimide (NHS)	Sigma-Aldrich corporation, India
4	1-ethyl-3-(3-dimethyl aminopropyl)carbodiimide (EDC)	Sigma-Aldrich corporation, India
5	Toluene	Avantor performance materials, India
6	Methanol	S.D. Fine chemicals , India
7	Dimethyl formamide (DMF)	Spectrochem Pvt. Ltd., India
8	Chitosan	Himedia chemicals, India
9	Folic acid	Sigma-Aldrich corporation, India
10	Ninhydrin	Sigma-Aldrich corporation, India
11	Dimethyl sulfoxide (DMSO)	Spectrochem Pvt. Ltd., India
12	Sodium hydroxide (NaOH)	Loba Chemie, India
13	Glacial acetic acid	Sisco research laboratories, India
14	Cystamine dihydrochloride	Sigma-Aldrich corporation, India

15	Potassium dihydrogen orthophosphate	Fischer Scientific, India
16	Sodium dihydrogen orthophosphate	Fischer Scientific, India
17	Glutathione (GSH)	Fischer Scientific, India
18	Sucrose	Loba Chemie, India
19	Potessium ethylenediaminetetraacetic acid (EDTA)	Fischer Scientific, India
20	Triton X100	Sigma-Aldrich corporation, India

Table 6.2: List of equipments used in the present work.

Sr. no.	**Equipment**	**Company Name and Place**
1	Digital weighing machine	Type AX 120,Shimadzu, Japan
2	Digital pH meter	Lab India instruments Ltd, India
3	Magnetic Stirrer	Remi equipment, India
4	Bath Sonicator	Fast clean ultra-cleaner, India
5	Hot air oven	Sedko laboratory equipments, India
6	Muffle furnace	Shreeji pharmaceutical scientific and laboratory equipments, India
7	UV visible spectrophotometer 1800	Shimadzu, Japan

8	Particle size analyser	Malvern Zetasizer, UK
9	FT IR Spectrophotometer	Shimadzu, Japan
10	Transmission electron microscope (TEM)	CM-200 Philips, India
11	Differential Scanning Calorimeter (DSC)	Shimadzu, Japan
12	BET Analyzer	ASAP 2020 V4.01 Surface Area Analyzer, Micromeritics, US
13	Spectrofluorimeter	Shimadzu, Japan
14	Incubator	JGUAN quality system, India
15	Centrifuge	Remi, India

Mesoporous silica nanoparticles (MSNs) are recognized for their ability to be chemically modified due to the presence of silanol groups. The modified surface of the mesoporous materials plays a vital role in the delivery of drugs. The major function of various surface modifications is their use to control the release of the drug based on particular stimuli or physiological conditions. Apart from this, different types of surface modification of MSNs undoubtedly improve the drug loading specifically for DNA and siRNA and also play a vital role in the delivery of drugs in suitable stimulated conditions. This is also favorable for the targeted delivery of drugs which improves the therapeutic efficiency of different cytotoxic drugs, as well as reduce their toxicity compared to the free drug.[1]

Two different pathways are available to functionalize the synthesized mesoporous silica nanoparticles:

The subsequent modification of the pore surface of a purely inorganic silica material ("grafting"),

The simultaneous condensation of corresponding silica and organosilica precursors ("cocondensation")

In the present work, post synthetic grafting method has been utilized because this method has the advantage that, under the synthetic conditions used, the mesostructure of the starting silica phase is usually retained.[2]

6.1 Synthesis of amino functionalized nanoparticles (MSN-NH_2 and CuO-MSN-NH_2):

Synthesis of MSN-NH_2 was carried out using anhydrous toluene as a solvent. The typical procedure used for the synthesis of MSN-NH_2 is as follows:

MSN (1.0 g) was dispersed in 80 ml of anhydrous toluene), and then APTES was added into this dispersion in 3 different proportions (0.25 ml, 0.5 ml and 0.75ml). The reaction mixture was refluxed for 20h to yield the 3-aminopropyl-functionalized MSN (MSN-NH_2). The resulting mixture was centrifuged at 10,000 rpm, the supernatant was discarded and the pellet was washed several times with methanol. Finally, the product obtained was dried overnight under vacuum at 45 ºC to obtain MSN-NH_2 as white precipitate.[3]

CuO-MSN-NH_2 was synthesized using the best suitable APTES concentration found for conjugation of APTES over MSN surface.

The modification of nanoparticles with APTES was confirmed by performing various analytical tests such as:

- Zeta potential
- FT-IR spectroscopy
- Ninhydrin test

  To determine primary amines content on the amine functionalized samples, ninhydrin colorimetric assay was performed as per the previously reported procedure with slight modifications: Briefly, small quantity (2mg) of amine-functionalized MSN were dispersed in 0.2 mL of methanol and sonicated to form homogenous dispersion. The

dispersion was allowed to react with 1 mL of ninhydrin solution (7.5 mg/mL) and placed in a boiling water bath for 15 minutes. The absorbance of the resulting solution was measured by UV-visible spectrophotometer at 581 nm.[4,5] The reaction of different known concentration of APTES with ninhydrin was applied for preparation of the calibration curve which was used for the quantification of amino groups .

6.2 Synthesis of MSN-COOH and CuO-MSN-COOH:

Carboxylation of MSNs and CuO-MSNs was performed by using succinic anhydride (SA) as per a previously reported procedure. In brief, 0.5 g of MSN-NH_2 as well as CuO-MSN-NH_2 were dispersed in 10 ml of anhydrous DMF, separately and sonicated for 10 min to homogenize the suspension. Then 10 ml of anhydrous DMF solution containing 3 g of SA was added to these suspensions. The reaction mixture was stirred at ambient temperature for 24 h. Finally, the resulting powders were washed with methanol and water for several times and dried overnight at 60º C and denoted as MSN-COOH and CuO-MSN-COOH.[6] The successful carboxylation of nanoparticles was confirmed by performing various analytical tests such as:

- Zeta potential
- FT-IR spectroscopy
- Ninhydrin test

6.3 Synthesis of chitosan-folic acid conjugate:

Conjugation of Folic acid to chitosan molecules was performed as per a previously reported procedure as follows: Equal moles of Folic acid and EDC were added to 20 mL anhydrous DMSO and stirred at room temperature until dissolved. The solution was then added slowly to 0.5% (w/v) chitosan in acetic acid aqueous solution (0.1 M, pH 4.7) and stirred at room temperature in the dark for 16 h. At the end of the reaction, the pH of the mixture was brought up to 9.0 by dripping with NaOH aqueous solution (1.0 M) and folic acid-chitosan conjugate was separated by centrifugation at 2500 rpm. The precipitate was first washed with

phosphate buffered saline (PBS, pH 7.4) and then with water several times. Finally, the folic acid conjugated chitosan was lyophilized.[7]

6.4 Drug loading and determination of entrapment efficiency:

The drug was loaded into MSN-NH_2 and CuO-MSN-NH_2 as follows:

50 mg of dry MSN- NH_2 and CuO-MSN-NH_2 were separately immersed in 25 ml of DOX aqueous solution (2 mg/mL in PBS of pH 5), and sonicated for 5 min to obtain a well dispersed suspension. After stirring for 24 h under light-sealed conditions, the DOX loaded nanoparticles (MSN-DOX as well as CuO-MSN-DOX) were centrifuged and washed with PBS (pH 5) several times. To evaluate the DOX loading efficacy, the supernatant was collected, and the residual DOX content was determined using a calibration curve of DOX by spectrofluorimetric measurement by exciting the samples at 480nm and measuring the intensity at emission wavelength of 556 nm.

The entrapment efficiency and drug loading efficiency was calculated using following formula:

$$\text{Entrapment Efficiency \%} = \frac{\text{Weight of Drug (DOX)in MSNs}}{\text{Weight of Drug (DOX) added initially}} * 100 \qquad (6.1)$$

$$\text{Loading Capacity \%} = \frac{\text{Weight of Drug (DOX)in MSNs}}{\text{Weight of Drug (DOX)} + \text{Weight of MSNs}} * 100 \qquad (6.2)$$

The same procedure was repeated using MSN-COOH and CuO-MSN-COOH and the drug loading was measured.

6.5 Formulation of DOX-MSN-SS-CH-FA and DOX-CuO-MSN-SS-CH-FA:

0.1 g of MSN-DOX were dispersed into 20 mL EDC/NHS mixture solution (EDC: 0.015 M, NHS: 0.015 M in PBS buffer pH=5). Then, 1g of cystamine dihydrochloride was added to the mixture and allowed to stir at room temperature for 24 h leading to formation of MSN-DOX-SS-NH_2.[8] Simultaneously, 250 mg CS-FA powder was dispersed in 50 mL (3%) acetic acid and stirred for 24 h. After 24 h the CS-FA solution (0.5%) was added into the solution

containing MSN-DOX-SS-NH_2 and allowed to stir at room temperature for 24 h in the dark. The CS-FA coated MSNs were collected by centrifugation at 10,000 and washed with deionized water several times before freeze drying.

6.6 In vitro stimuli mediated drug release study:

In vitro drug release patterns from 5mg DOX suspension and various DOX loaded formulations such as DOX-MSN, DOX-MSN-CH-FA, DOX-MSN-SS-CH-FA, DOX-CuO-MSN, DOX-CuO-MSN-CH-FA and DOX-CuO-MSN-SS-CH-FA (5mg DOX equivalent) were studied using a activated dialysis dialysis membrane having molecular weight cut off 12000, average flat width of 29.31 mm, average diameter of 17.5 mm and approximate capacity of 2.41 ml/cm, purchased from Himedia Laboratories Pvt. Ltd.

In vitro drug release was carried out using two different media, phosphate buffer pH 7.4 and phosphate buffer pH 5.5, in the presence or absence of GSH (10mM). Samples were dispersed in 1 ml diffusion medium and taken in activated dialysis bag which was placed in a beaker containing 50 mL of diffusion media with 100 RPM magnetic stirring. 1 ml samples were withdrawn periodically and replaced with the same volume of fresh dissolution medium at predetermined time intervals up to 120h. The amount of drug released was determined by performing spectrofluorimetric analysis as described earlier.

6.7 Hemolysis study:

For hemolysis assay, the red blood cells (RBCs) were isolated from chicken blood obtained from government approved slaughter house. Fresh blood was collected in dipotassium EDTA treated tubes and plasma was removed as supernatant by centrifugation at 3000 rpm for 10 min. The RBCs pellet was refined by successive rinsing with PBS buffer (pH 7.4). The suspension of RBC was diluted 10 times with PBS buffer (pH 7.4), and then 200 µL of RBCs suspension was added to 800 µl of free DOX and DOX loaded formulations such as DOX-MSN, DOX-MSN-SS-CH-FA, DOX-CuO-MSN, and DOX-CuO-MSN-SS-CH-FA with different concentration (0.1 - 100 µg/ml). For positive control, 200 µl of RBCs suspension was added to 800 µl Triton X100 (2% v/v), and for negative control, 200 µl of RBCs suspension was added to 800 µl of PBS buffer (pH 7.4). Afterwards, all of the samples were

incubated for 2 h in a shaker incubator. Finally, the samples were centrifuged at 10,000 rpm for 2 min, and the absorbance of supernatant (hemoglobin) was measured by UV-visible spectrophotometer at 398 nm. The hemolytic activity percentages of the different samples were calculated as follows:[9]

$$\% \text{ Hemolysis} = \frac{\text{Abs(sample)} - \text{Abs(ctrl} -)}{\text{Abs(ctrl} +) - \text{Abs(ctrl} -)} * 100 \qquad (6.3)$$

6.8 Results and discussions:

6.8.1 Synthesis of MSN-NH_2 and CuO-MSN-NH_2:

The reaction to synthesize amino functionalized nanoparticles was carried out using anhydrous toluene as a solvent due to the fact that the presence of water causes hydrolysis and autocondensation of aminosilanes and forms new, discrete moieties. Furthermore, aqueous solvent also encourages the clustering of the silanes which ultimately leads to non-uniform distribution of amino group, majorly populated at the pore entrance. This uneven distribution significantly reduces the surface area and thereby also affect the drug loading. On the other hand, anhydrous solvents can provide uniform distribution of amino groups with high density due to formation of strong hydrogen bonds in anhydrous non-polar solvent.[10]

Figure 6.1 represents the change in zeta potential of MSNs observed with change in the concentration of APTES. As the concentration of APTES in the reaction increases, zeta potential also increases. This gradual change in the zeta potential towards positive charge upon reaction with APTES confirmed the successful conjugation of APTES with MSNs. Addition of 0.75 ml of APTES was capable of producing MSN-NH_2 with good positive surface charge (+ 6.45 mV). Hence, CuO-MSN-NH_2 was synthesized by adding 0.75 ml of APTES in the reaction and the zeta potential of synthesized CuO-MSN-NH_2 was found to be +9.8 mV.

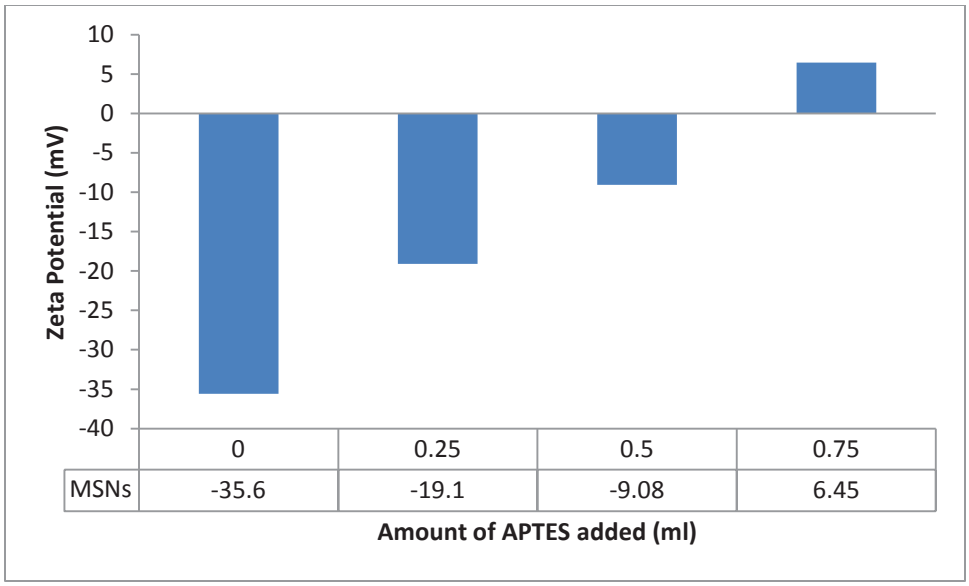

Figure 6.1: Change in the zeta potential of MSNs with change in the amount of APTES added.

The success of amino functionalization over MSNs and CuO-MSNs surface was further confirmed by FT-IR spectroscopic analysis. Figure 6.2 A compares the FT-IR spectrum of MSN before and after amino functionalization while figure 6.2 B compares the FT-IR spectrograms of CuO-MSNs and CuO-MSN-NH_2. The absorption signal shown by MSNs at 1068 representing the stretching vibration of Si-O-Si was retained after amino functionalization also. An additional absorption peak near 1543 was observed in case of MSN-NH_2 which was not present in plain MSN. This additional peak might be due to presence of -NH_2 bending. Similarly in case of CuO-MSN-NH_2, all the absorption peaks of CuO-MSN were retained but an addition peak was observed near 1539 representing -NH_2 bending which wasn't present in CuO-MSNs before reacting with APTES. This addition of peak confirmed that a reaction took place between MSNs or CuO-MSNs and APTES and amino group was successfully grafted over the surface of these nanoparticles.

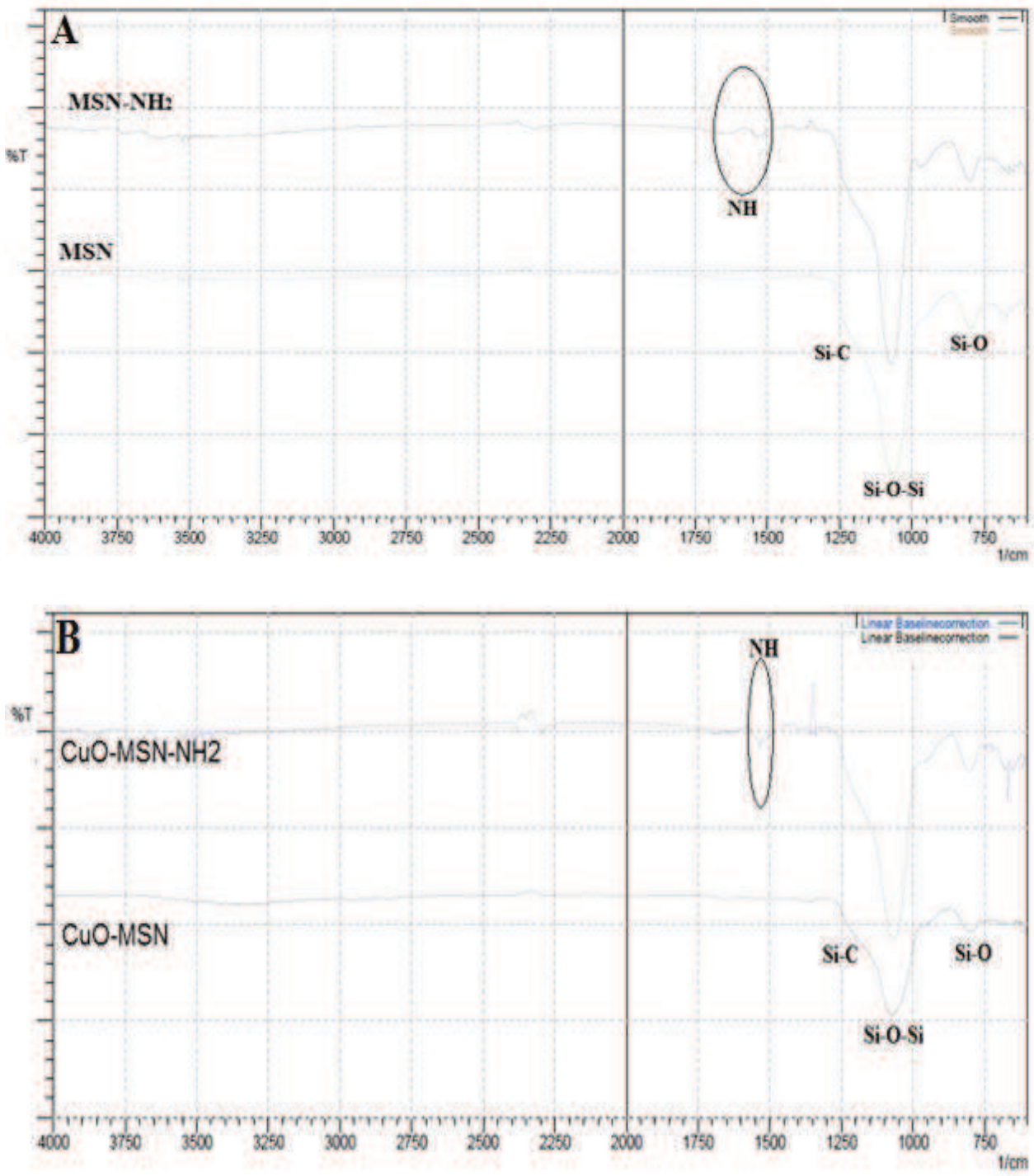

Figure 6.2: FTIR spectrum before and after amino functionalization of MSNs (A) and CuO-MSNs (B).

Both the gradual increase in zeta potential and the presence of -NH_2 absorption peaks in FTIR spectrum confirmed the successful animo functionalization over MSNs and CuO-MSNs surface. Later ninhydrin test was performed to quantify the amount of APTES conjugated to the said nanoparticles. Ninhydrin reagent is frequently used to measure the free amines in the biochemical synthesis due to the fact that it forms Ruhemann's purple upon reacting with free amines which provide characteristic UV-Vis absorption peak.

The amount of APTES conjugated to MSNs was about 61.8% while it was about 60.4% in case of CuO-MSNs. Thus, ninhydrin test further confirmed the success of amino functionalization of nanoparticles and also quantified the degree of functionalization.

6.8.2 Synthesis of MSN-COOH and CuO-MSN-COOH:

Amino functionalized MSNs and CuO-MSNs underwent reaction with succinic anhydride in order to achieve carboxyl groups over the surface of nanoparticles.

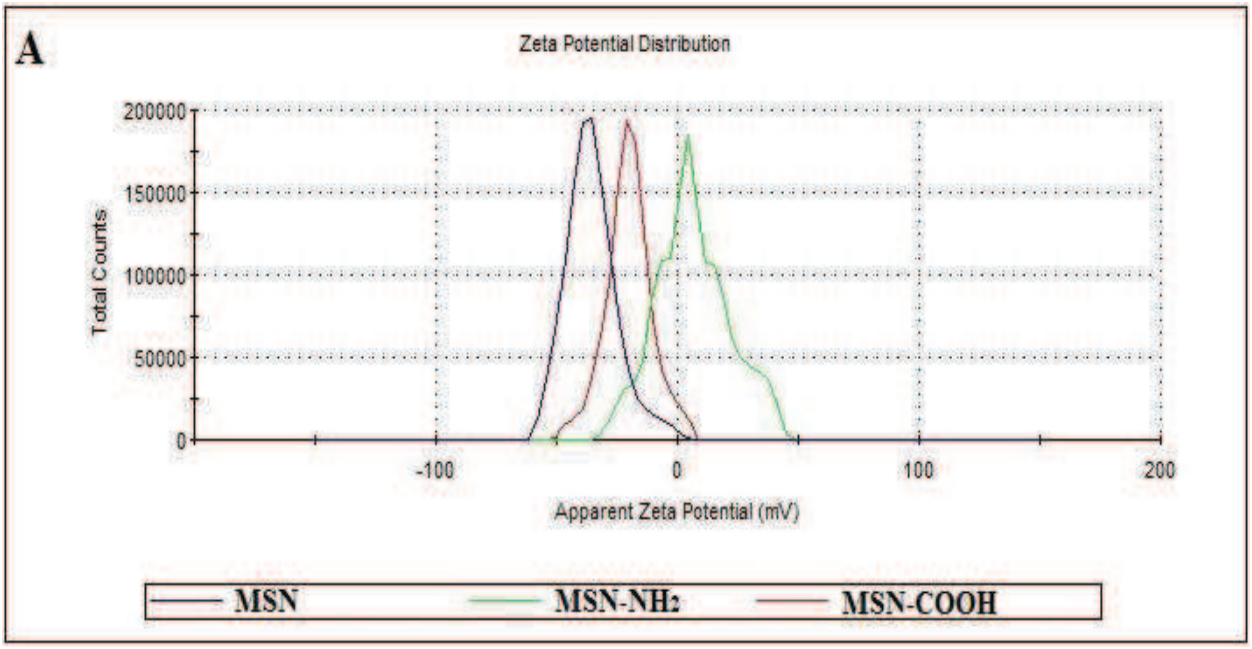

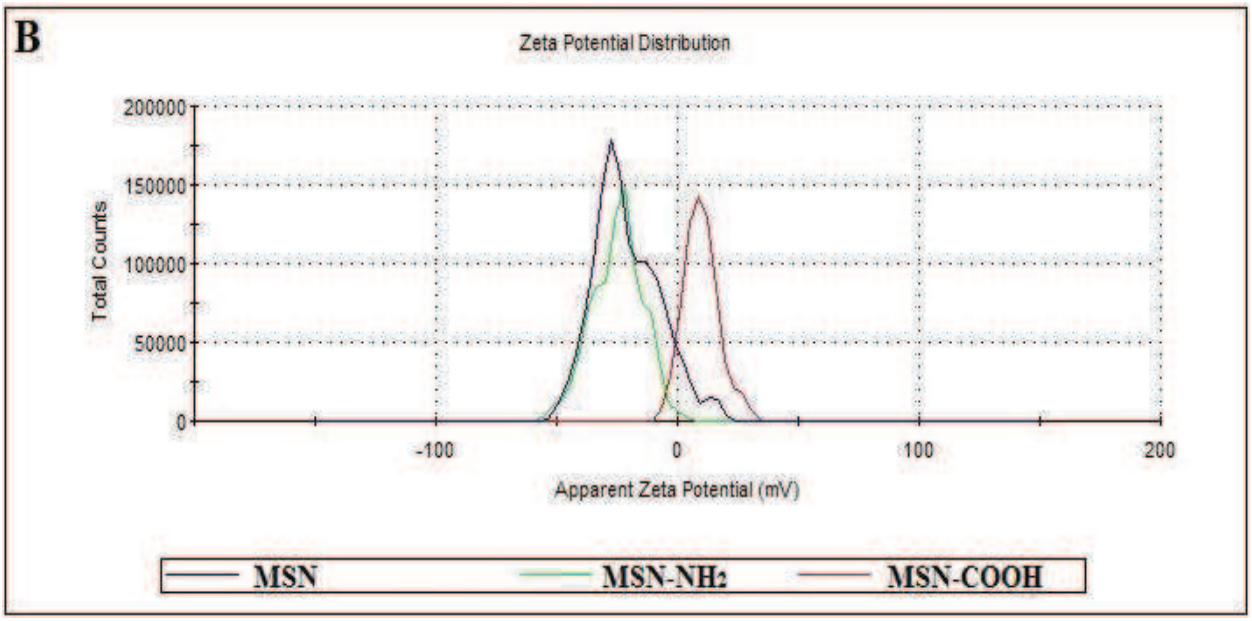

Figure 6.3: Change in the zeta potential before and after each functionalization of MSN (A) and CuO-MSN (B).

As seen in figure 6.3 A, the zeta potential of MSNs was negative initially due to high density of silanol groups which was increased and became positive after functionalization with APTES. The zeta potential again decreased to great extent and became negative upon reaction with succinic anhydride (-20.2 mV). This decrease in the zeta potential might be due to successful carboxylation over MSNs' surface. Similarly, the zeta potential of CuO-MSN was negative initially and successful amino functionalization made it positive. This positive charge again became negative after reaction with succinic anhydride (-24.9 mV) proving accomplishment of COOH attachment over CuO-MSN.

The successful grafting of COOH group over MSN and CuO-MSN was further supported by FTIR spectrum of carboxyl functionlized nanoparticles. As seen in figure 6.4 A, an additional characteristic absorption peak near 1710 cm^{-1} was observed in case of MSN-COOH while characteristic absorption peak near 1704 cm^{-1} was added in CuO-MSN-COOH (Figure 6.4 B) representing carbonyl group (C=O). This additional peak observed confirmed the presence of COOH group in the synthesized MSN-COOH and CuO-MSN-COOH.

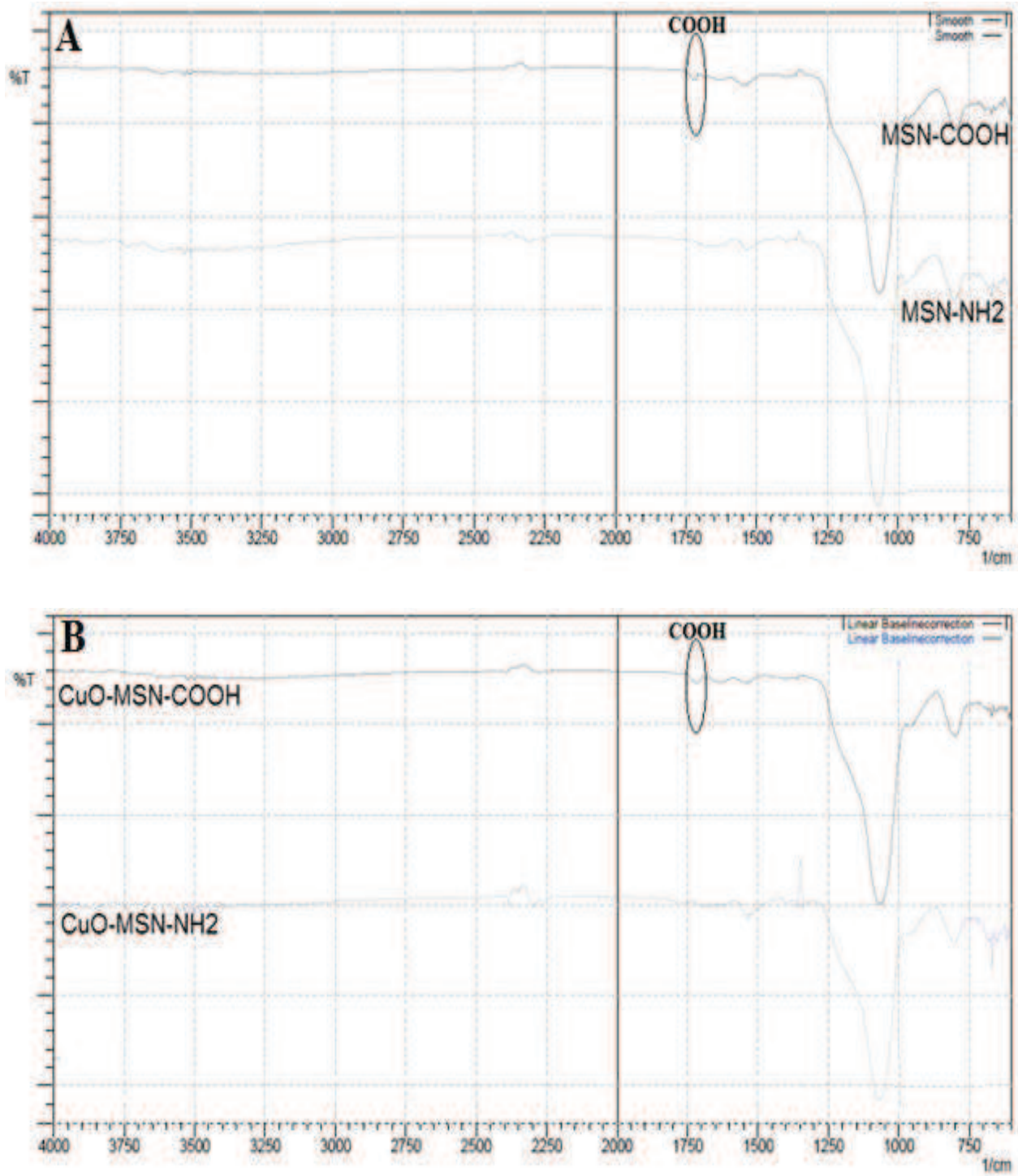

Figure 6.4: FTIR spectrum before and after carboxyl functionalization of MSN-NH_2 (A) and CuO-MSN-NH_2 (B).

Table 6.3 showed the results obtained by performing ninhydrin test. As seen in the table, reaction of MSNs with APTES was successful and about 60% of APTES added was conjugated over the surface of nanoparticles. After the reaction with succinic anhydride, a considerable decrease in the number of free amino group was noticed. This decrease might be due to reaction of free amino groups with SA and thereby formation of carboxyl functionalized nanoparticles. Almost 50% of the amino groups were reacted with SA to produce carboxylic groups.

Table 6.3: Amount of amino groups measured by performing ninhydrin test after each modification.

Sr. No.	Type of nanoparticles	Percent APTES Conjugated	Percentage of conjugated amino groups converted to carboxylic group
1	MSNs	61.8	54.7
2	CuO-MSNs	60.4	56.3

6.8.3 Drug loading:

The selected drug DOX was initially loaded into amino functionalized nanoparticles (MSN-NH_2 and CuO-MSN-NH_2). As seen in table 6.4, the drug loading observed in MSN-NH_2 and CuO-MSN-NH_2 was very less. As seen in figure 6.5, DOX carries positive charge (pKa 8.2[11]), due to which electrostatic repulsion between DOX molecules and amino functionalized nanoparticles might have taken place leading to less loading of DOX. As compared to MSN-NH_2, the drug loading was much higher in case of CuO-MSN-NH_2 which might be due to presence of negatively charged CuO in the MSN framework.

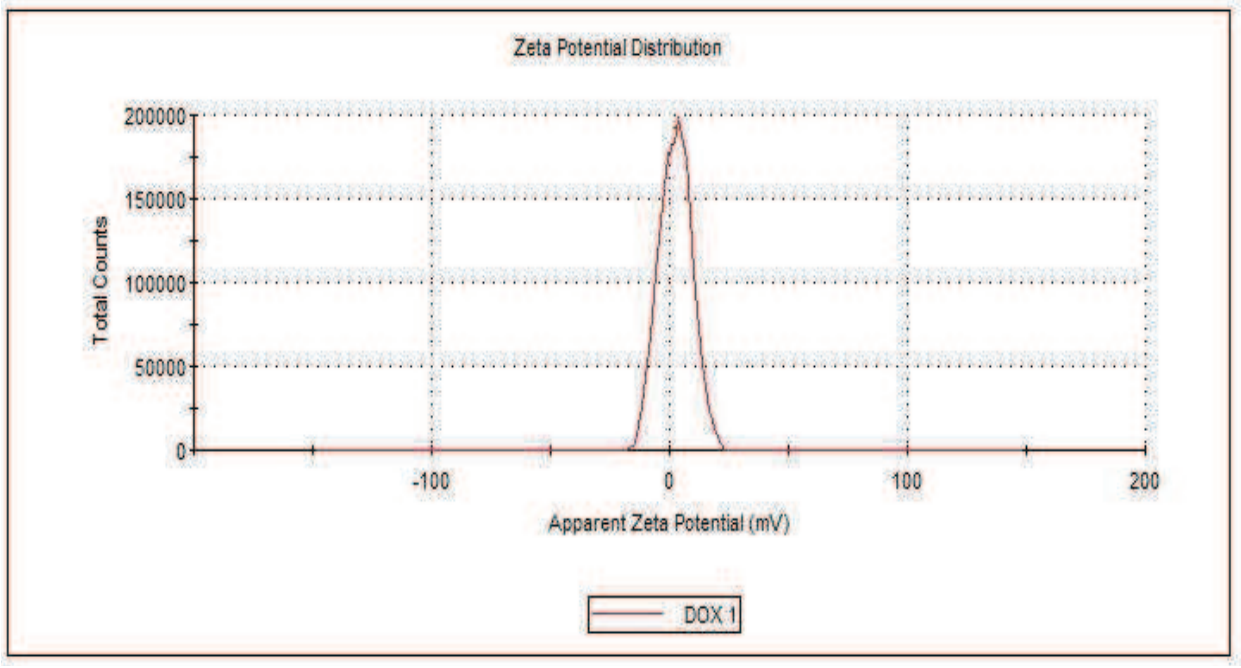

Figure 6.5: Zeta potential of DOX.

Because of the less drug loading into amino functionalized nanoparticles, the carboxyl group containing MSN-COOH and CuO-MSN-COOH were used for improving the loading of DOX and a significant increase in the loading efficiency was observed. So, it can be said that, DOX can be loaded more into negatively charged particles as DOX is positively charged.

Table 6.4: DOX loading in differently functionalized MSNs.

Sr. No.	Type of functionalized nanoparticles	Loading capacity (%)
1	MSN-NH2	8.12
2	CuO-MSN-NH2	16.8
3	MSN-COOH	31.94
4	CuO-MSN-COOH	43.6

Figure 6.6 represents the DSC thermograms of plain DOX, DOX-MSNs and DOX-CuO-MSNs. As seen in the image, DSC thermogram of pure DOX showed sharp endothermic peak at 229.24 °C which is the melting point of DOX. Neither DOX-MSN nor DOX-CuO-MSN showed melting point peak of DOX confirming the complete incorporation of DOX into the pores of nanoparticles.

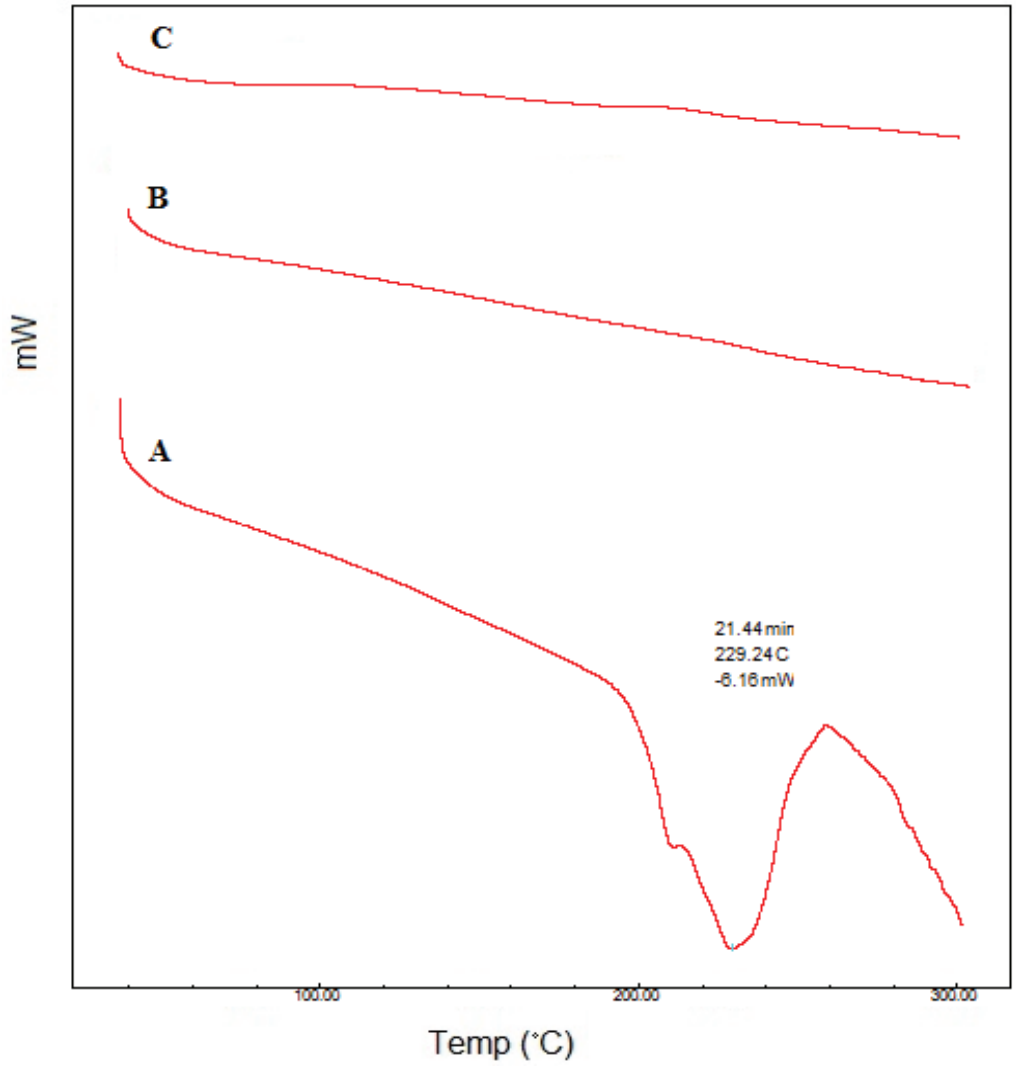

Figure 6.6: DSC thermogram of DOX (A), DOX-MSN (B) and DOX-CuO-MSN.

6.8.4 Synthesis of CH-FA conjugate:

Most of the anticancer drugs including DOX, are known to cause severe toxicity to normal cells making the need of stimuli responsive cancer cell targeted nanoparticles, capable of targeting cancer cells and releasing the drug molecule at target site only with minimum premature drug released, highly desirable.

A natural cationic polysaccharide, chitosan (CH), composed of β-(1-4)-linked glucosamine units, together with some N-acetyl-d-glucosamine unit, is known to hold a great potential in various biomedical applications because of its favorable properties such as biodegradation, nontoxic nature and antibacterial activity. Apart from this, within a specific range of pH, the amino groups of CH can be protonated which opened a direction for designing the formulation/nanocarriers that can be responsive to external pH-stimuli of cancer cells.[12]

Being vitamin in nature, folic acid (FA), do not exhibit any deleterious effect to normal cells. FA possess various favorable properties like small size, low cost, ready availability, less immunogenic and most importantly targeting capability due to highly over expressed folate receptors over breast cancer cells which make FA a primary choice as a targeting moiety for breast cancer.[13]

Because of the above mentioned advantages, CH was selected to cap the surface of drug loaded MSNs while FA was selected as a targeting moiety. Both CH and FA were conjugated using carbodiimide reaction and the amount of folate conjugated to CH was measured using UV-visible spectroscopy as described in chapter 3. About 66.58% of FA was found to be attached to CH to form CH-FA conjugate.

Figure 6.7 represents the FTIR spectrum of synthesized CH-FA conjugate. As seen in the spectrum, a characteristic absorption peak near 1711 cm^{-1} was observed which might be representing the carbonyl (C=O) functional group. At the same time, peak near 1516 was observed corresponding to amide (N-H) bending. Furthermore, a sharp peak at 3506 stands for amine (N-H) stretching. The presence of carbonyl and amide group in the

FTIR spectrum confirmed the formation of -CONH group. So, it can be said that the FA was conjugated successfully with the CH.

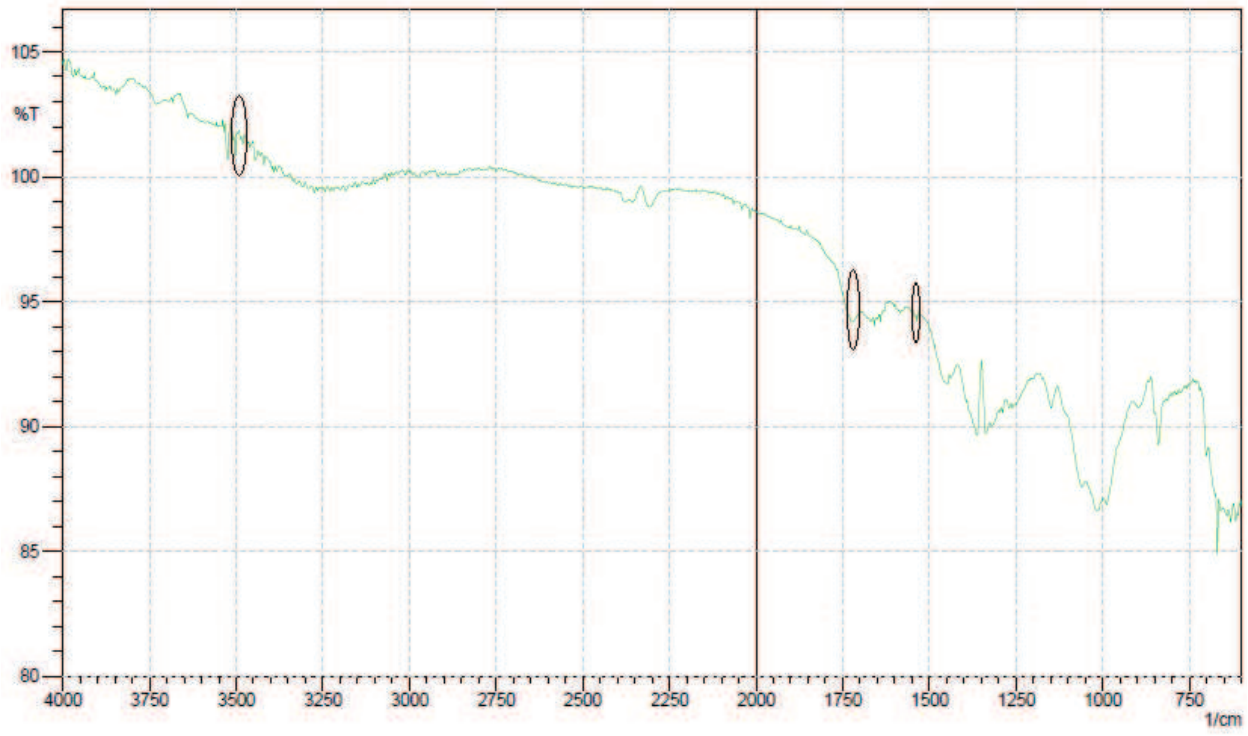

Figure 6.7: FTIR spectrum of CH-FA conjugate.

6.8.5 Characterization of DOX-MSN-SS-CH-FA and DOX-CuO-MSN-SS-CH-FA:

The DOX loaded MSNs and CuO-MSNs were reacted with cystamine dihydrochloride to incorporate disulfide bond on surface and then capped with the CH-FA conjugate.

As seen in the figure 6.8, the CH-FA capping considerable increased the size of MSNs and CuO-MSNs. The particles size of synthesized MSNs was about 113 nm which was raised to 149.8 nm after capping with CH-FA while that of CuO-MSN was about 144 nm which increased to 186 nm. Though, there was a significant increase in the particles size, DOX-MSN-SS-CH-FA and DOX-CuO-MSN-SS-CH-FA were smaller than the cut-off size of tumor neovasculature pores which make them amenable to accumulate in cancer cells by the enhanced permeation and retention (EPR) effect that is responsible for passive targeting to tumor tissues.

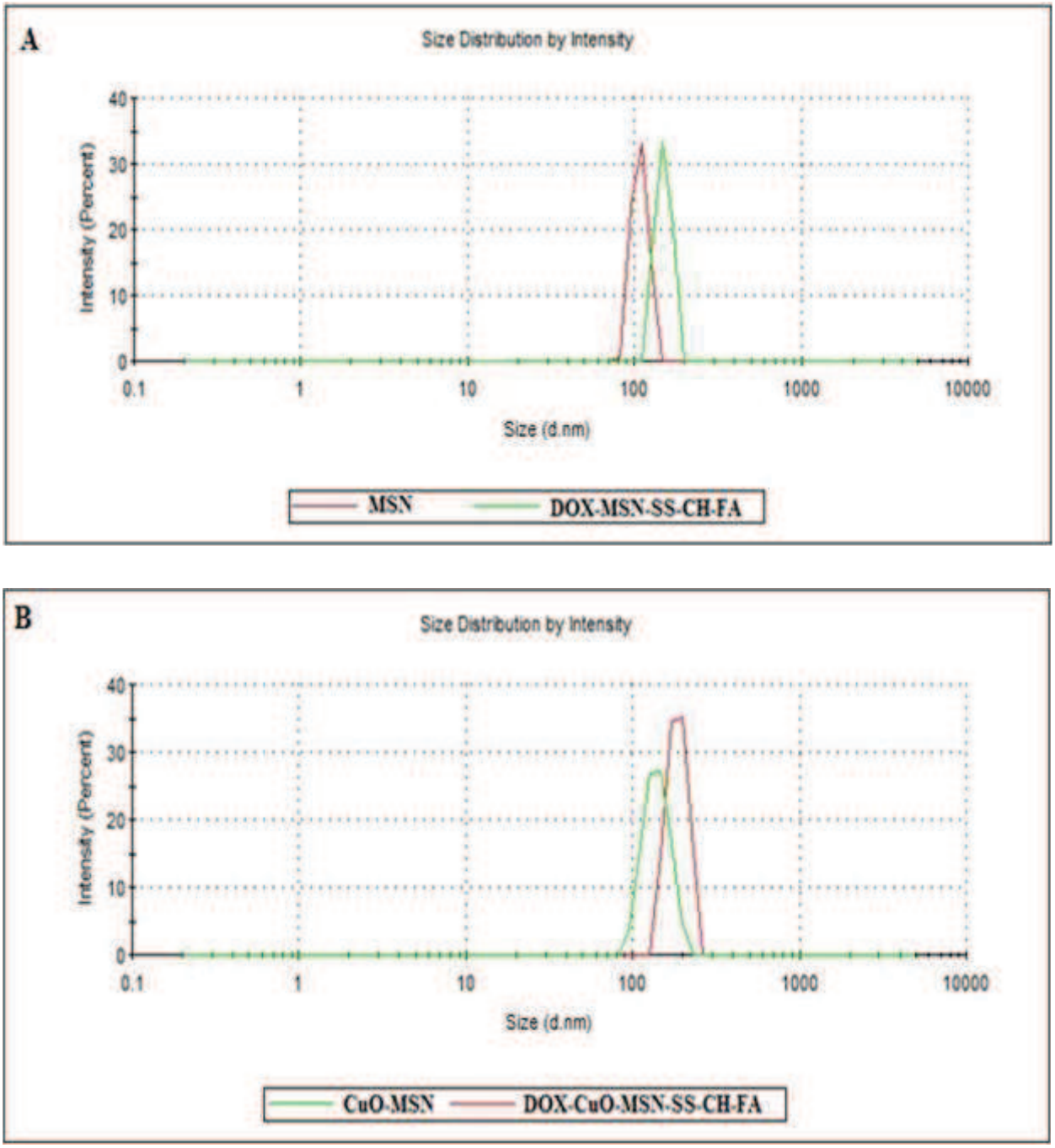

Figure 6.8: Change in the particle size of MSN (A) and CuO-MSN (B) after capping with CH-FA conjugate via disulfide bond.

Figure 6.9 represents the zeta potential of DOX-MSN-SS-CH-FA and DOX-CuO-MSN-SS-CH-FA. As seen in the figure, MSN-COOH and CuO-MSN-COOH were found to possess negative zeta potential of about -20.2mV and -24.9 mV, respectively. After capping with CH-FA via disulfide bond, the zeta potential of these particles raised and became positive (14.2mV and 16.6mV from -20.2mV and -24.9mV, respectively). This shift towards the positive charge confirmed the capping of CH-FA conjugate over nanoparticles surface as chitosan molecules possess high positive charge due to large number of amino groups.

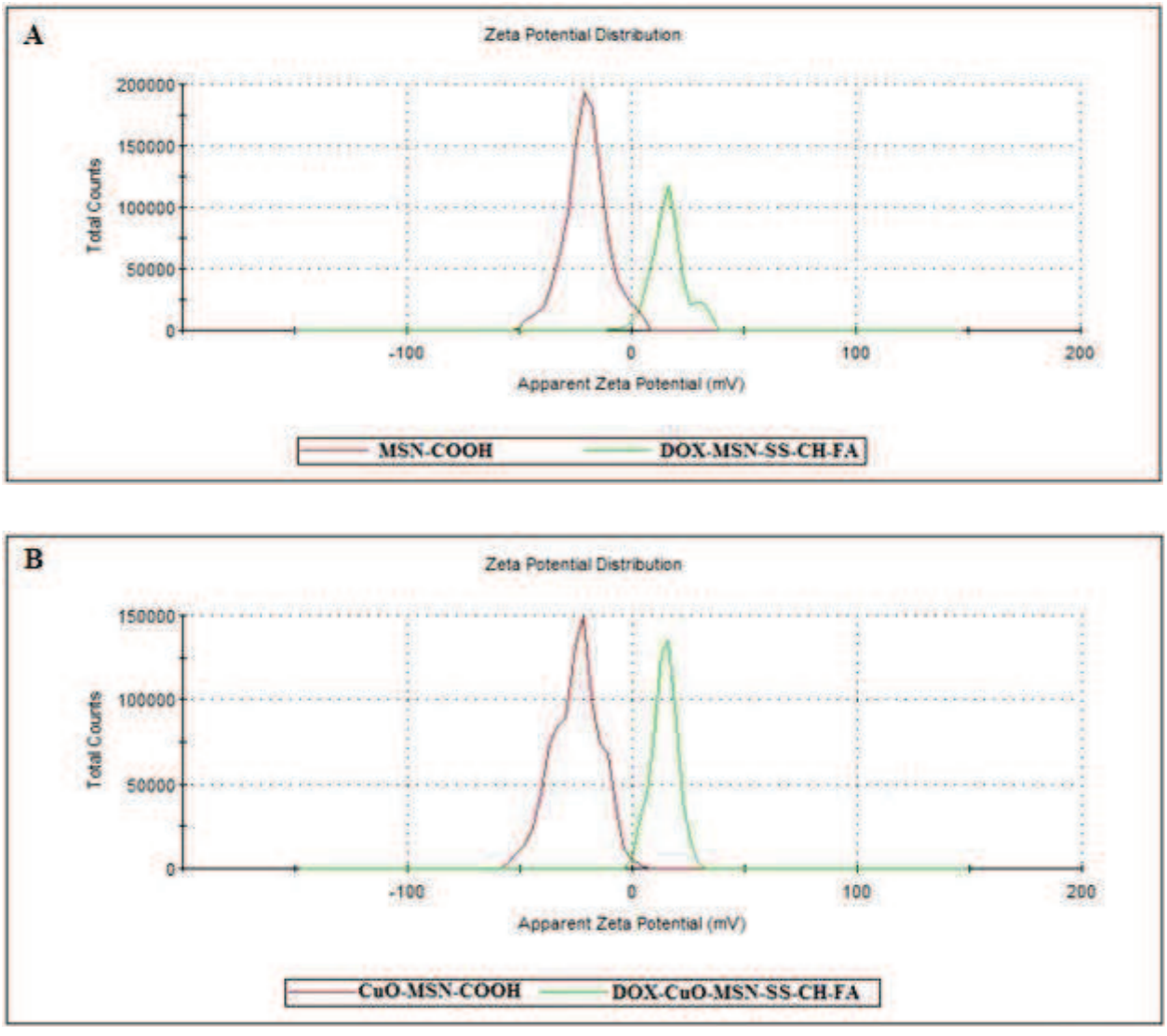

Figure 6.9: Change in the zeta potential of MSN-COOH (A) and CuO-MSN-COOH (B) after capping with CH-FA conjugate via disulfide bond.

Figure 6.10 stands for TEM images of DOX-MSN-SS-CH-FA and DOX-CuO-MSN-SS-CH-FA. As seen in the images, a distinguished CH-FA shell around the core MSNs and CuO-MSNs was observed proving successful capping of CH-FA over MSNs. Furthermore, the ordered pores are not seen in the images proving that the pores were filled with DOX and/or blocked by CH-FA capping. The corresponding selected area electron diffraction (SAED) pattern shown clearly demonstrated amorphous structure of CH-FA capped nanoparticles.

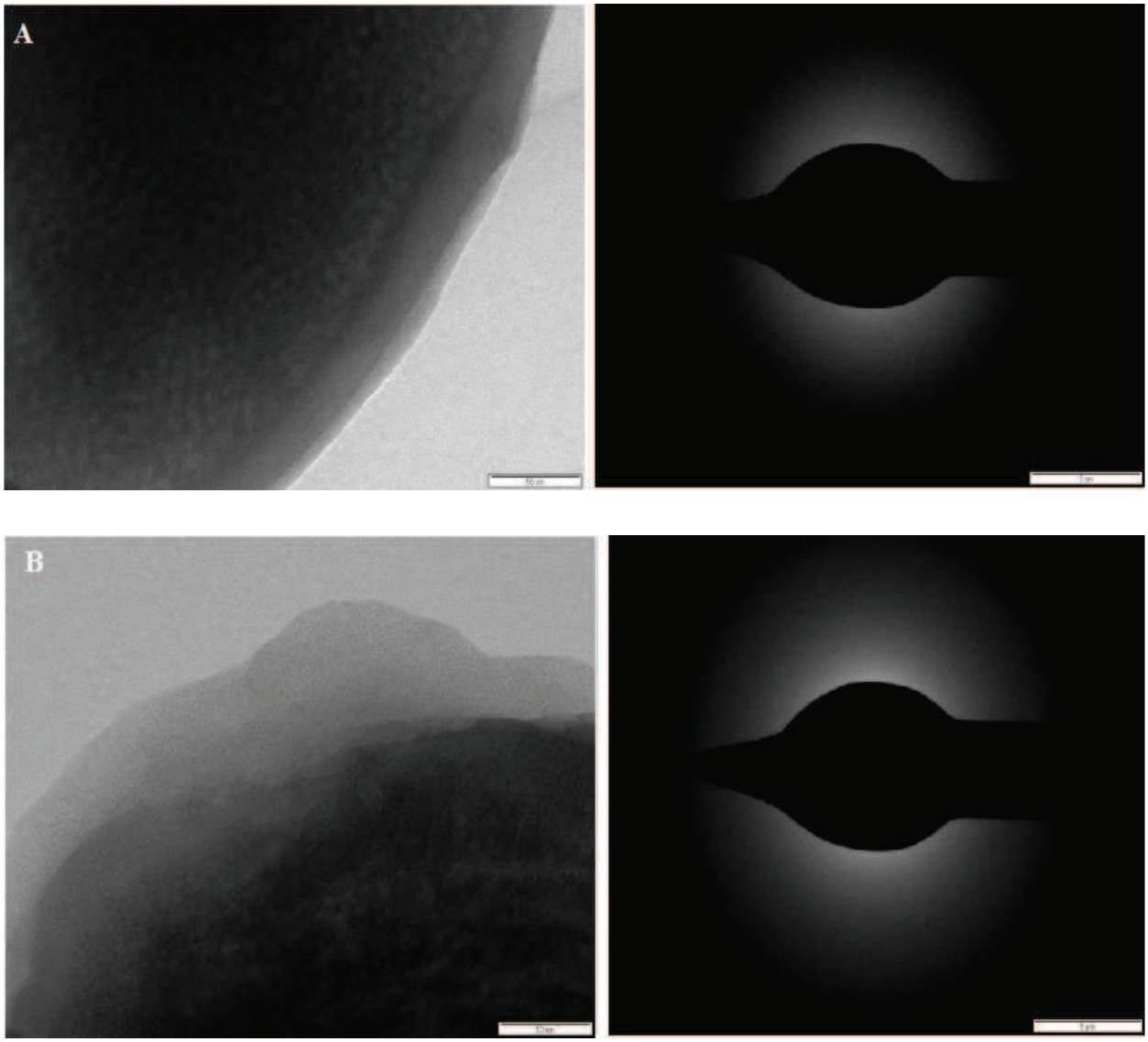

Figure 6.10: TEM and SAED images of DOX-MSN-SS-CH-FA (A) and DOX-CuO-MSN-SS-CH-FA (B).

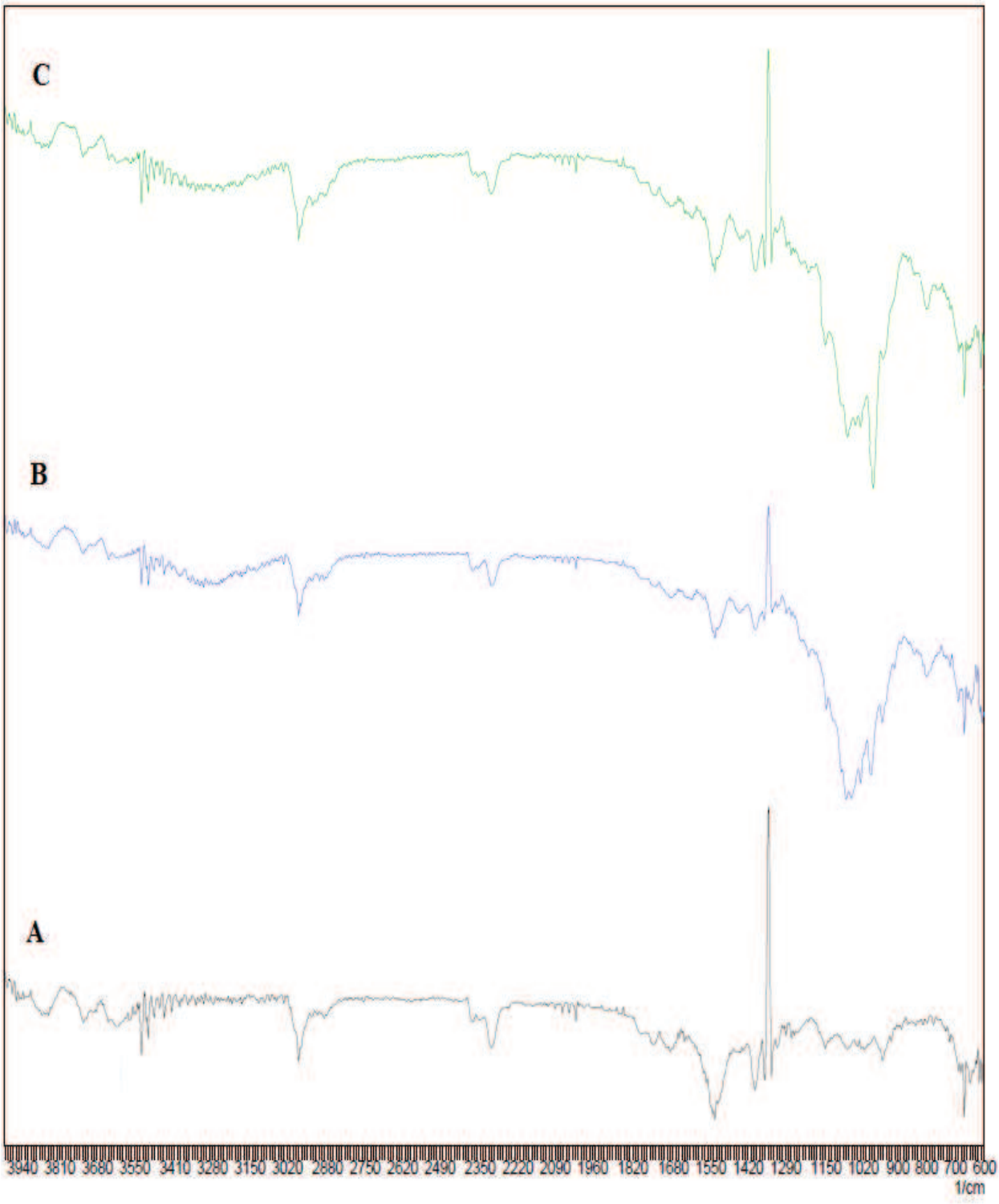

Figure 6.11: FTIR spectrum of: CH-FA conjugate (A), DOX-MSN-SS-CH-FA (B) and DOX-CuO-MSN-SS-CH-FA (C).

The FTIR spectrum of DOX-MSNs and DOX-CuO-MSNs after capping with CH-FA conjugate was recorded and shown in figure 6.11. As seen in image, both DOX-MSN-SS-CH-FA and DOX-CuO-MSN-SS-CH-FA showed all the characteristic absorption peaks of CH-FA such as a peak near 1742 cm^{-1} represent the carbonyl group (C=O), peak near 1500 cm^{-1} correspond to amide (N-H) bond bending while the amine (N-H) bond stretching vibrations were observed near 3400 cm^{-1}. The presence of all the characteristic peaks of CH-FA in DOX-MSN-SS-CH-FA and DOX-CuO-MSN-SS-CH-FA confirmed the success of capping process.

It has been well documented that the polymer based nanoparticles are taken up by cells through the endocytosis-lysosome pathway. The lysosymes possess slightly acidic pH because of the proton pumps on the lysosome membrane. The extracellular pH of normal tissues and blood is approximately 7.4, whereas low pH conditions are considered a hallmark of malignant solid tumor tissues. The pH of a tumor microenvironment is between 6.0 and 7.0, which is mainly caused by high glycolysis rate and high level of CO_2. Intracellular organelles, such as endosomes (pH=5.5) and lysosomes (pH<5.5) show further drop in a pH value as compared to the extracellular microenvironment of a tumor.[14,15] Apart from this, the tumor cells acquire about 1000 times higher redox potential than the extracellular environment.[16] In order to validate the premature drug release blocking effectiveness, pH responsiveness of CH-FA capping, and redox responsive cleavage of disulfide bond, in vitro drug release experiment for different types of MSNs and CuO-MSNs was performed in four discrete media having two different pH of 7.4 and 5.5 representing biological environment (bloodstream) and endocytic compartment, respectively, and the presence and absence of 10mM GSH.

As seen in figure 6.12, plain DOX got released completely within 3 hours in all the media. The DOX-MSN and DOX-CuO-MSN also showed drug release comparable to plain DOX and complete DOX was released within 5 hours. Change in pH or presence of GSH didn't make any significant difference in the drug release from non coated particles. All the other formulations controlled DOX release for prolonged time period. DOX-MSN-CH-FA and DOX-CuO-MSN-CH-FA showed increased drug release under acidic environment while DOX-MSN-SS-CH-FA and DOX-CuO-MSN-SS-CH-FA demonstrated highest drug release in phosphate buffer with pH 5.5 containing 10mM

GSH. The release of DOX from DOX-MSN-SS-CH-FA and DOX-CuO-MSN-SS-CH-FA was in the following order.

PBS 5.5 +10 mM GSH > PBS 7.4 + 10 mM GSH > PBS 5.5 > PBS 7.4

The higher drug release in presence of 10mM GSH can be attributed to the cleavage of disulfide bond by GSH.

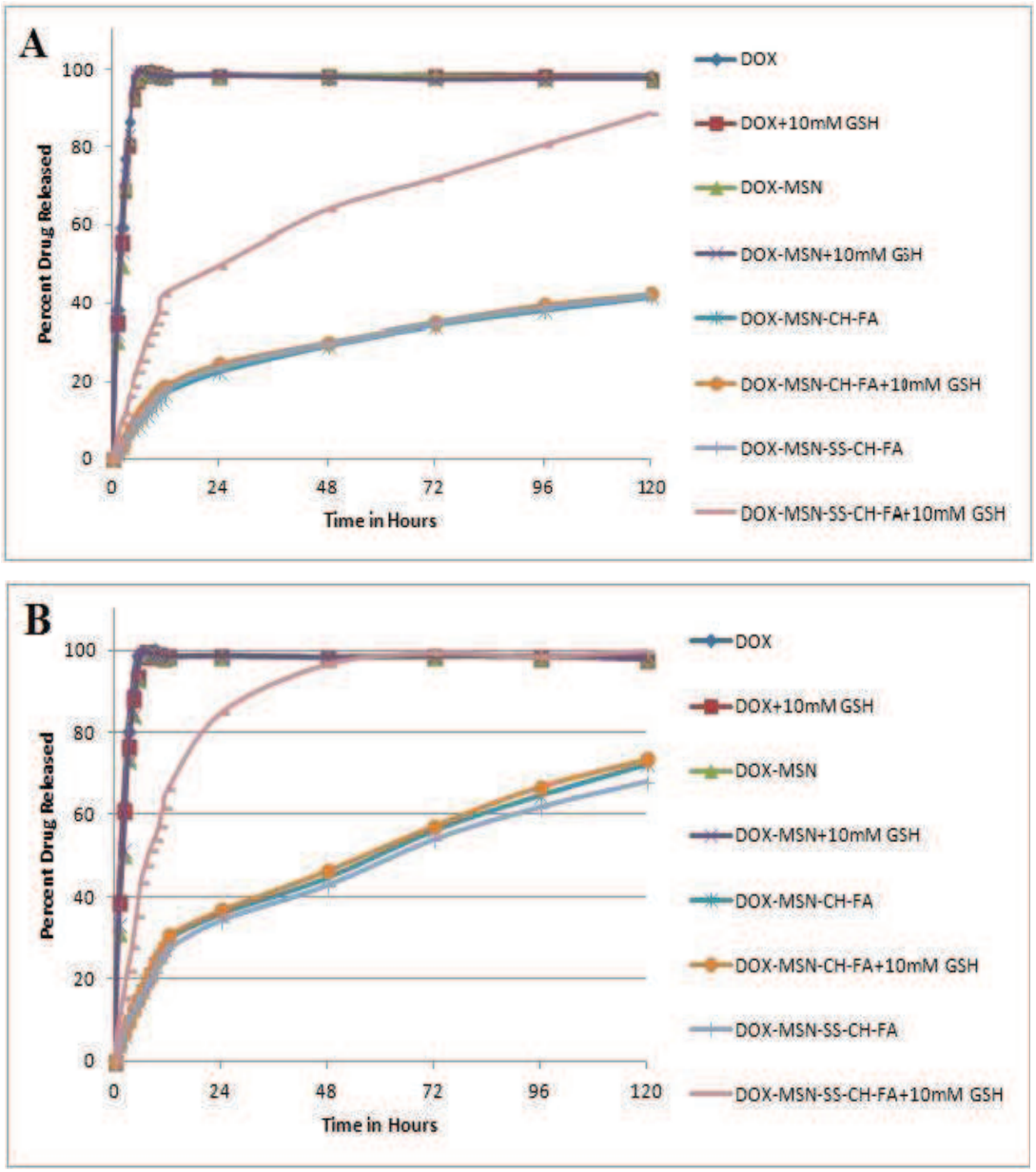

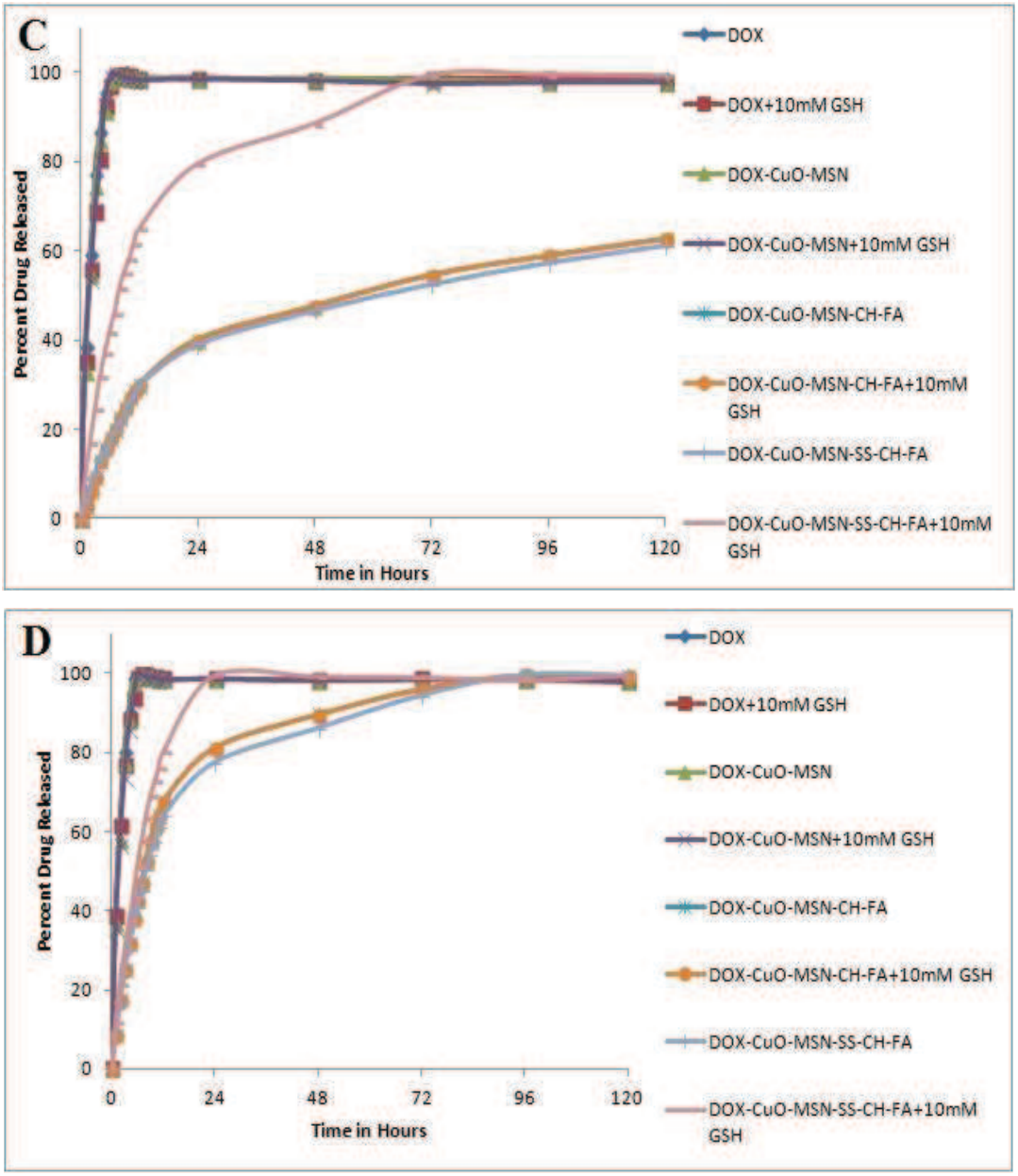

Figure 6.12: In vitro drug release study of: Different DOX-MSN samples in phosphate buffer pH 7.4 (A) and phosphate buffer pH 5.5 (B) and Different DOX-CuO-MSN samples in phosphate buffer pH 7.4 (C) and phosphate buffer pH 5.5 (D) with or without 10mM GSH.

To sum up, the designed drug delivery system exhibited a dual responsive (pH-sensitive and redox responsive) nature and sustained DOX release behavior which is of critical significance for selective and efficient treatment of diverse types of cancers.

Hemocompatibility of functionalized drug loaded nanoparticles was confirmed by performing the in vitro hemolysis study and the effect of plain drug and various drug formulations was checked on the erythrocytes. Figure 6.13 depicts change in the percent hemolysis as a function of increasing concentration of DOX.

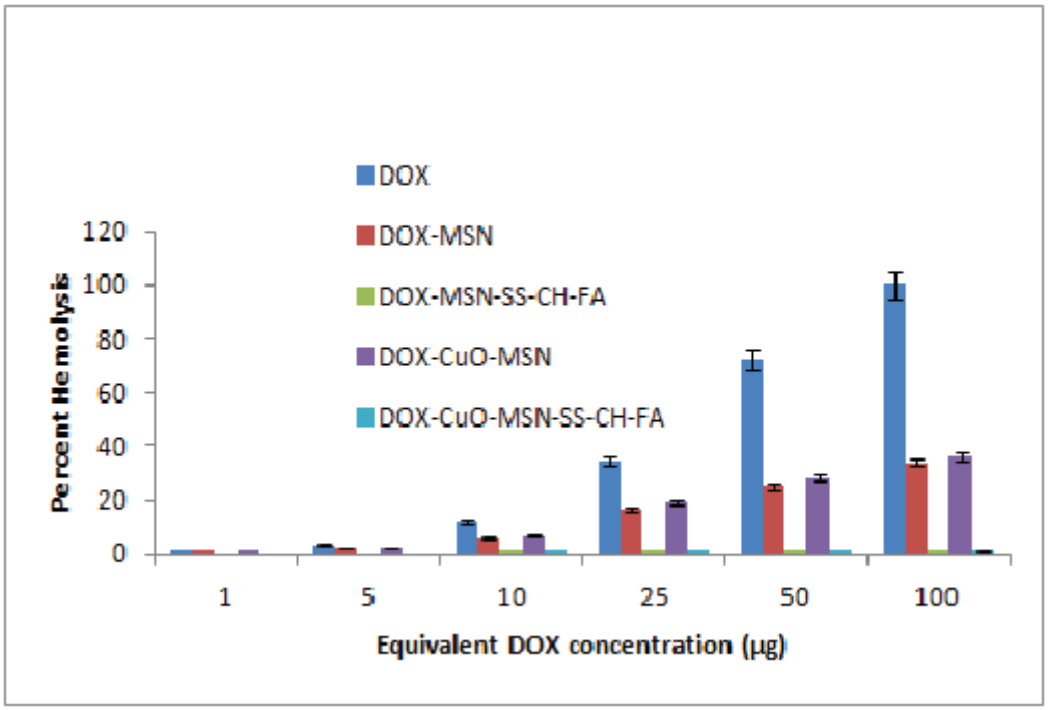

. **Figure 6.13:** Hemolytic activity of DOX and different DOX loaded formulations.

As seen in the figure, as the concentration of DOX increased, the percent hemolysis increased. At higher concentration, plain DOX caused almost 100% hemolysis. The incorporation of DOX into MSNs and CuO-MSNs showed considerable reduction in percent hemolysis but it was also not sufficient as more than 30% hmolysis was observed. This must be due to fast release of DOX and its interaction with erythrocytes. As compared to these, DOX-MSN-SS-CH-FA and DOX-CuO-MSN-SS-CH-FA showed very less hemolysis even at highest concentration of DOX. It proved that the CH-FA capping significantly reduced hemolysis and increased the biocompatibility of DOX loaded MSNs and CuO-MSNs.

References:

1. Natarajan SK, Selvaraj S. Mesoporous silica nanoparticles: importance of surface modifications and its role in drug delivery. RSC Advances. 2014, 4:14328-14334.
2. Hoffmann F, Cornelius M, Morell J, Froba M. Silica based mesoporous organic-inorganic hybrid materials. Angewandte chemie. 2006, 45:3216-3251.
3. Friedman M. Applications of the Ninhydrin Reaction for Analysis of Amino Acids, Peptides, and Proteins to Agricultural and Biomedical Sciences. Journal of Agricultural and Food Chemistry. 2004, 52:385-406.
4. Bottom CB, Hanna SS, Siehr DJ. Mechanism of the ninhydrin reaction. Biochemical Education. 1978, 6:4-5.
5. Yoncheva K, Popova M, Szegedi A, Mihaly J, Tzankov B. Functionalized mesoporous silica nanoparticles for oral delivery of budesonide. Journal of Solid State Chemistry 2014, 211:154-61.
6. Zhang J, Niemela M, Westermark J, Rosenholm JM. Mesoporous silica nanoparticles with redox-responsive surface linkers for charge-reversible loading and release of short oligonucleotides. Dalton Transactions. 2014, 43:4115-26.
7. Daryasari MP, Akhgar MR, Mamashli F, Bigdeli B, Khoobi M. Chitosan-folate coated mesoporous silica nanoparticles as a smart and pH-sensitive system for curcumin delivery. RSC Advances. 2016, 6:105578-88.
8. Luo Z, Cai KY, Hu Y, Zhao L, Liu P. Mesoporous silica nanoparticles end-capped with collagen: redox-responsive nanoreservoirs for targeted drug delivery. Angewandte Chemie. 2011, 50:640–643.
9. Golla K, Cherukuvada B, Ahmed F, Kondapi AK. Efficacy, Safety and Anticancer Activity of Protein Nanoparticle-Based Delivery of Doxorubicin through Intravenous Administration in Rats. 2012, 7(12):e51960.
10. Bruhwiler D. Postsynthetic functionalization of mesoporous silica. Nanoscale. 2010, 2:887-892.
11. Shahabi S, Doscher S, Ballhorst T, Treccani L, Maas M, Dringen R, Rezwan K. Enhancing cellular uptake and doxorubicin delivery of mesoporous silica nanoparticles via surface functionalization: effects of serum. Applied Materials and Interfaces. 2015 7(48): 26880-26891.

12. Hu X, Wang Y, Peng B. Chitosan-Capped Mesoporous Silica Nanoparticles as pH-Responsive Nanocarriers for Controlled Drug Release. Chemistry An Asian Journal. 2014, 9(1):319-327.
13. Narayanan S, Binulal NS, Mony U, Manzoor K, Nair S, Menon D. Folate targeted polymeric green nanotherapy for cancer. Nanotechnology. 2010, 21:1-13.
14. Xiao D, Jia HZ, Zhang J, Liu CW, Zhuo RX, Zhang XZ. A Dual-Responsive Mesoporous Silica Nanoparticle for Tumor-Triggered Targeting Drug Delivery. Small. 2014, 10(3):591-598.
15. Duo Y, Li Y, Chen C, Liu B, Wang X, Zeng X, Chen H. DOX-loaded pH-sensitive mesoporous silica nanoparticles coated with PDA and PEG induce pro-death autophagy in breast cancer. RSC Advances. 2017, 7:39641-50.
16. Jiao J, Li X, Zhang S, Liu J, Di D, Zhang Y, Zhao Q, Wang S. Redox and pH dual-responsive PEG and chitosan-conjugated hollow mesoporous silica for controlled drug release. Material Science and Engineering C. 2016, 67:26-33.